ANGIOGRAPHNET: REAL-TIME PREDICTION OF VESSEL EXPANSION IN CORONARY ANGIOPLASTY USING GEOMETRIC DEEP LEARNING

PAYAL CHANDAK AND KARIM KADRY

Abstract. Coronary atherosclerosis can impede blood flow in the heart, necessitating revascularization procedures such as angioplasty. Coronary angioplasty success relies on the complex interplay between stent deployment and patient-specific micro-morphology. To facilitate intervention planning, we propose a graph convolutional neural network (GCNN) that leverages geometric deep learning for real-time prediction of vessel expansion based on the 3D arterial structure. This approach significantly reduces computational time, enabling the use of a surrogate model to optimize coronary interventions, enhancing decision-making processes, and improving patient outcomes in time-sensitive clinical settings.

Key words. Computational Cardiology, Medical Imaging, Machine Learning, Numerical Simulation, Virtual ANgioplasty, Graph Convolutional Networks

1. Introduction. Coronary artery disease (CAD) remains the foremost global cause of mortality, primarily attributed to the buildup of atherosclerotic plaque within the coronary wall, which subsequently leads to reduced blood flow to the heart muscle[8]. These plaques exhibit a wide variety of micro-anatomical phenotypes, with their complex micro-morphology and micro-topology significantly impacting the efficacy of clinical interventions [10]. To restore blood flow and alleviate the detrimental effects of CAD, coronary angioplasty is performed. This revascularization procedure involves the insertion and expansion of a stent within the artery, with its success hinging on the intricate interaction between the device and the patient's unique coronary micro-morphology, such as the presence of calcium deposits [2].

Cardiologists currently base their interventional decisions on invasive and non-invasive imaging technologies, such as optical coherence tomography (OCT), to analyze plaque composition and determine stent size, placement, inflation pressure, and vessel preparation techniques [7]. While OCT provides high-resolution, 3D image stacks of atherosclerotic lesions, enabling the differentiation of various plaque components based on their optical appearance, relying solely on these broad morphological indicators may not provide adequate information to predict device success [3, 13]. Consequently, understanding and utilizing 3D micro-anatomical information to guide percutaneous coronary intervention (PCI) strategies is of paramount importance to optimize clinical outcomes.

Computational cardiology endeavors to address this limitation by converting intravascular 3D OCT images of coronary arteries into patient-specific, multi-material digital twins. These digital representations serve as the foundation for virtual angioplasty simulations, which predict vessel expansion in response to stent deployment parameters[3, 13]. These simulations employ partial differential equations to model the complex interplay of soft tissue biomechanics, contact mechanics, and metal alloy plasticity. However, while highly accurate, such numerical simulations are time-consuming and computationally intensive, preventing their use in catheter labs, where critical interventional parameter decisions are made within minutes of obtaining intravascular images.

To bridge this gap, recent advancements in scientific machine learning have fostered the development of surrogate machine learning models, trained on numerical simulation data, to predict the dynamic state of organic physical systems more rapidly than traditional numerical simulations [9]. This paves the way for real-time applications in clinical settings. Previous surrogate models for PDEs primarily relied on convolutional neural networks (CNNs), which were limited by their inability to handle non-Euclidean data, non-homogeneous prediction resolutions, and low resolutions[11]. In contrast, graph-based approaches predict system dynamics using a graph representation of computational meshes, which serve as the substrate for numerical simulations. These approaches accommodate anisotropic resolutions and non-Euclidean data handling, offering a more versatile solution for complex, patient-specific geometries[11].

In this course project, we propose leveraging graph convolutional neural networks (GCNN) to predict vessel expansion in coronary angioplasty based on the morphological representation of 3D arterial structures. This approach would significantly reduces the time taken to predict vessel response, enabling the use of a real-time surrogate model for optimizing coronary interventions. By providing a more comprehensive understanding of the intricate interactions between cardiovascular morphology and device-based interventions, our proposed GCNN has the potential to accelerate decision-making processes and patient outcomes in coronary angioplasty. With this novel methodology, cardiologists will be better equipped to tailor interventions to individual patients, resulting in more successful revascularization procedures and improved long-term prognosis. Our contributions are therefore as follows:

- We develop a parametric model of calcified coronary arteries to produce meshes with different morphological parameters
- We develop and leverage a virtual angioplasty platform that numerically simulates stent expansion to calculate vessel displacement
- We introduce a novel method of condensing the three-dimensional atherosclerotic morphology onto a 2D mesh manifold embedded in three dimensions, which preserves the information necessary to predict vessel expansion in response to virtual angioplasty
- We leverage a graph convolutional architecture to take the manifold representation of a coronary artery to predict nodal displacements on the inner surface.
- We trained and validated our graph convolutional network on numerical simulations of virtual angioplasties applied to a wide range of coronary morphologies.

2. Methodology.

In the methodology section of our study, we delineate the systematic process undertaken to evaluate the practicality of employing Graph Neural Networks (GNNs) in predicting the outcomes of virtual stent angioplasty procedures. The methodology comprises of several phases: 1) constructing the computational models for virtual stenting (section 2.1), 2) the implementation of virtual stent angioplasty simulations (section 2.3), 3) the generation of training data for the GNN (section 2.4), 4) the development of the GNN architecture (section 2.5),and 5) the conduction of validation experiments section (section 2.6).

2.1. Computational Models.

2.1.1. Baseline Geometries.

The virtual angioplasty platform consists of three components, a computational model of a calcified coronary artery, a stent, and a balloon. The stent has a nominal (starting) diameter of 3mm, is 20mm long and has a radial thickness of 70μm. The multi-folded angioplasty balloon measures 23mm in length and has an outer diameter of 0.9mm. It is designed with a nominal diameter of 3mm. The baseline arterial model is partitioned into three distinct segments, two of which represent healthy sections located at either extremity, and one diseased segment positioned centrally. The healthy sections are configured to have a cylindrical geometry with a diameter of 2.9mm, a thickness of 0.66mm, and a length of 40mm. In these healthy portions, the media and adventitia layers are respectively 0.32mm and 0.34mm thick, adhering to the empirical data obtained from the analysis of 13 fresh human cadaveric hearts by Holzapfel et al [6]. Interposed between these healthy portions is the diseased segment, characterized by a stenosis degree of 60%. This value was derived from an in-depth analysis of an Optical Coherence Tomography (OCT) pullback from a patient diagnosed with Coronary Artery Calcification (CAC).

2.1.2. Parametric variations of the artery model.

The parametric variations of the artery can be seen in Figure 1. Lumen stenosis diameter (L) ranges from 0 to 2, the calcium thickness (T) ranges from 0.1mm to 2mm, and calcium arclength (A) span from 10 to 360 degrees.

2.1.3. Meshing.

The artery was meshed with first order tetrahedra. The number of elements varies between the different cases but is usually on the order of 100,000. The balloon has meshed with 9600 4-node quadrilateral membranes. The stent has been meshed with 266,588 first order linear bricks

2.2. Material Properties.

2.2.1. Artery properties.

The artery was defined as hyperelastic/plastic and the properties were obtained from Poletti et. al [12]. The hyperelastic behaviour is modeled as a polynomial strain energy function:

$$\psi = C_{10}(I_1-3) + C_{20}(I_1-3)^2 + C_{30}(I_1-3)^3 + C_{40}(I_1-3)^4 + C_{50}(I_1-3)^5 + C_{60}(I^1-3)^6 \tag{2.1}$$

Where, C_{xx} are the material coefficients, and I_1 is the first invariant of the cauchy deformation tensor. The hyperelastic coefficients for the plastic and elastic behaviour can be found in Tables 1 and 2.

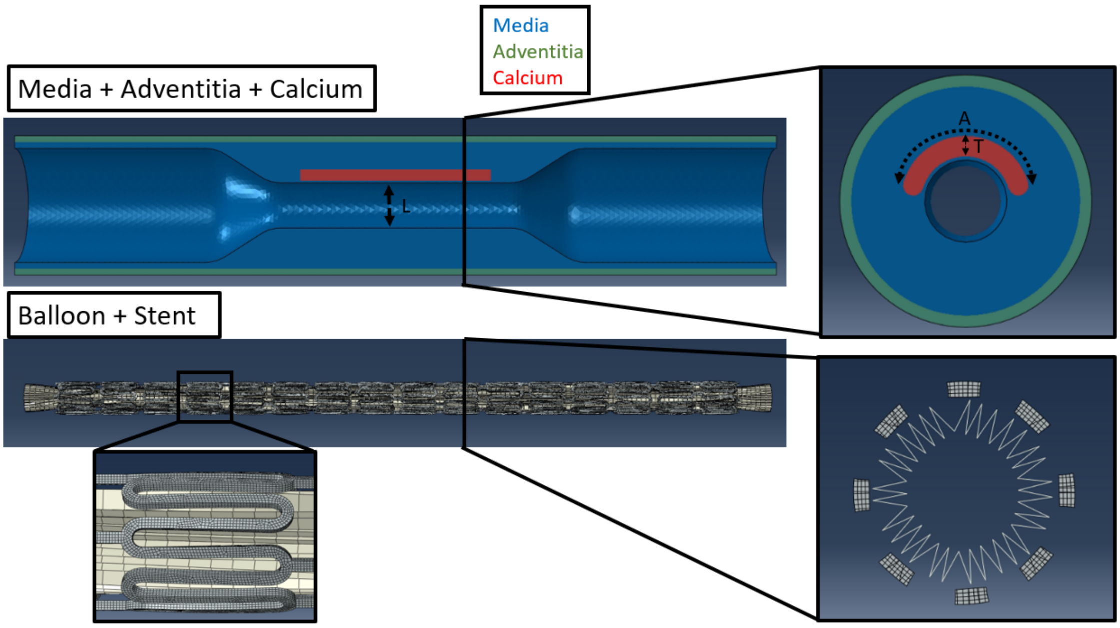

Fig. 1: A visual representation of the computational models for virtual angioplasty. Top row: Longitudinal inset of parametrized geometry of calcified coronary artery, which consists of media (blue), adventitia (green) and embedded calcified plaque (red). Right inset shows cross section of artery with associated calcium deposit. Bottom row: balloon+stent angioplasty system after crimping operation, left inset shows zoom in on crimped stent mesh, right inset shows cross section of balloon folding pattern.

	C_{10}	C_{20}	C_{30}	C_{40}	C_{50}	C_{60}
Adventitia	2.60×10^{-1}	4.76×10^{1}	-4.09×10^{3}	5.29×10^{5}	-2.69×10^{7}	5.65×10^{8}
Media	7.29×10^{-2}	3.71×10^{0}	-1.56×10^{2}	9.18×10^{3}	-2.61×10^{5}	2.91×10^{6}

Table 1: Hyperelastic Behavior of Artery Tissue

2.2.2. Balloon and Stent Properties. The balloon was assumed to have a first order Ogden hyperelastic behavior (Table 3:

$$\Psi = \frac{\mu_1}{\alpha_1}\left(\lambda_1^{\alpha_1} + \lambda_2^{\alpha_1} + \lambda_3^{\alpha_1} - 3\right) \tag{2.2}$$

Where λ_X are the principle stretches along each direction. The stent was assumed to have an elastic-plastic material behavior as can be seen in tables 4 and 5.

2.3. Virtual Angioplasty.

2.3.1. Crimping procedure. The stent was initially 3D-drawn at its nominal diameter of 3 mm to match the standard received by cardiologists. However, coronary arteries can vary in diameter from 3.7 mm to 1.9 mm. Therefore, in order to deliver the stent through these arteries, it needs to be crimped or compressed.

To achieve crimping, 16 rigid planes were placed in an orthoradial pattern, maintaining a distance equal to the stent radius. This arrangement ensures immediate contact from the beginning of the simulation. To effectively crimp the stent, a radial displacement to a diameter of 1.1 mm was imposed on the crimping planes. This process reduces the stent diameter, enabling it to pass through the coronary arteries. The resulting configuration represents the final crimped stent.

2.3.2. Inflation and Deflation. In the simulation setup, both the proximal and distal ends of the artery and balloon are pinned, meaning they can rotate locally but not translate. The

Artery Tissue	Plastic Strain (-)	Plastic Stress (MPa)
Adventitia	0	1.60
	0.07	2.30
	0.40	4.00
Media	0	0.70
	0.07	1.10
	0.40	2.00

Table 2: Plastic Behavior of Artery Tissue

μ_1 (MPa)	α_1 (-)
80	-15

Table 3: Hyperelastic behavior of the Balloon

balloon is inflated with a pressure of 1.4 MPa. The length of the stent was intentionally chosen to overlap a portion of each healthy end of the artery, ensuring that the stent spans the entire length of the lesion. Once the balloon is inflated, it is then correspondingly deflated, leaving only the stent to keep it open.

In terms of contact behavior, tangential contact is assumed to be frictionless, while normal contact is assumed to be hard, meaning no penetration is allowed. These contact properties were applied between every part of the model. Considering the highly non-linear dynamics of this simulation, which includes contact and significant deformation, Abaqus/Explicit (Abaqus Inc., Providence RI, USA) was utilized for the analysis. Abaqus/Explicit is well-suited for such simulations due to its ability to handle explicit dynamics and large deformation scenarios. We run each simulation on a node with 28/40 cpus and 128 GB of ram, we utilize domain parallelization, which divides the computational mesh into seperate domains for each cpu, and loop paralellization, which utilizes multiple cpus to quickly solve certain parallelizable loop procedures. Figure 2 demonstrates the results of a single stent angioplasty procedure

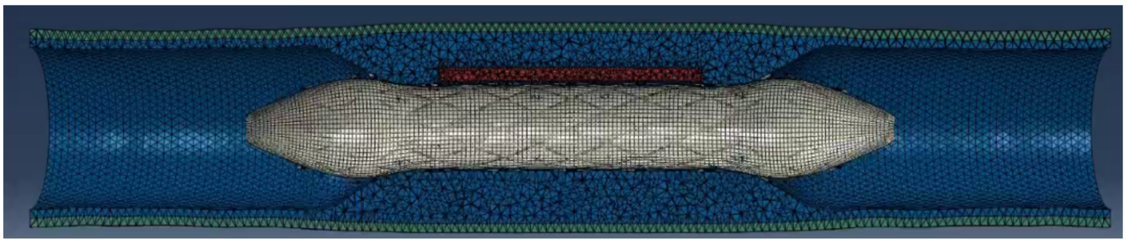

Fig. 2: A visual representation of a virtual stent angioplasty at the end of the inflation step.

2.4. Production of Training Data. The virtual angioplasty produces a a vector prediction of the displacement at every node in the mesh. While this mesh and the nodewise displacement vector can be fed into the graph neural network, they prove quite large to process on GPU's. We therefore instead choose to project the 3D calcium onto the luminal surface of the artery mesh. Producing a 2D triangular mesh embedded in 3D space. We project the calcium by shooting 1 ray per node from the surface of the lumen in an outwardly radial fashion. We measure the thickness of the calcium by finding the intersection points between the nodal rays and calcium elements. We then assign each node a thickness value. Similarly, we found the xyz displacement vector associated with each node on the surface. This can be visualized in figure 3

2.5. Geometric Deep Learning.

2.5.1. Problem definition. We define vessel expansion as a node-level displacement prediction problem. We are given as input a 2D surface mesh that is a homogeneous graph $G = (\mathcal{V}, \mathcal{E})$

Young's modulus (GPa)	Poisson's ratio (-)
203	0.3

Table 4: Elastic Behavior of the stent

Plastic stress (MPa)	Plastic strain (-)
203	0.3
480	0
1208	0.35
1300	0.62
2300	1.09

Table 5: Plastic behavior of the stent

with nodes in the vertex set $v_i \in \mathcal{V}$, edges $e_{i,j} = (v_i, v_j)$ in the edge set $\mathcal{E}$, where v_i is called the head/source node and v_j is called the tail/target node. Each node also has an initial embedding, which we denote as $\mathbf{h}_i^{(0)}$, that contains various expertly curated features. For each node, we would like to predict a two-dimensional vector $\mathbf{h}_i^{(n)} = (x, y)$ that represents the displacement of mesh at that node in the respective coordinate directions.

2.5.2. Message passing in graph convolutional layers. Given a graph of an artery, we aim to learn a numerical vector $\mathbf{h}_i^{(n)} = (x, y)$ for each node such that it captures vessel expansion at that point in a manner that is physiological sound and consistent with other parts of the artery. This is achieved by transforming initial node embeddings through several layers of local graph-based non-linear function transformations to generate predictions [5]. These functions are optimized iteratively, given a loss function to gradually minimize the error of making poor vessel expansion predictions. Upon convergence, optimized functions generate an optimal set of node displacements.

Step 1: Initialization. We denote the input node embedding $\mathbf{X}_i$ for each node i, which is initialized using curated features such as the thickness of calcium at the node, and the position of the node. For every layer l of message-passing, there are the following three stages:

Step 2: Propagating relation-specific neural messages. We calculate a transformation of the embedding at each node from the previous layer $\mathbf{h}^{(l-1)}$, where the first layer $\mathbf{h}^{(0)} = \mathbf{X}$. This is achieved via applying a weight matrix $\mathbf{W}_M^{(l)}$ on the previous layer's embedding:

$$\mathbf{m}_i^{(l)} = \mathbf{W}_M^{(l)} \mathbf{h}_i^{(l-1)}$$

Step 3: Aggregating local network neighborhoods. For each node v_i, we aggregate on the incoming messages $\{\mathbf{m}_j^{(l)} | j \in \mathcal{N}_i\}$ from neighboring nodes denoted as $\mathcal{N}_i$ by taking the average of these messages:

$$\widetilde{\mathbf{m}^{(l)}}_i = \frac{1}{|\mathcal{N}_i|} \sum_{j \in \mathcal{N}_i} \mathbf{m}_j^{(l)}$$

Step 4: Updating network embeddings. We then combine the node embedding transformed from the previous layer and the aggregated messages to obtain the new node embedding:

$$\mathbf{h}_i^{(l)} = \mathbf{h}_i^{(l-1)} + \widetilde{\mathbf{m}^{(l)}}_i$$

After L layers of propagation, we arrive at our encoded node embeddings $\mathbf{h}_i^{(L)}$ for each node i. The final node embeddings $\mathbf{h}_i^{(N)}$ represent the displacement prediction at the given node.

2.5.3. Graph U-Net Architecture. We employ the Graph U-Net architecture [4], inspired by the conventional U-Net architecture [14] for image segmentation. This Graph U-Net architecture effectively captures and decodes hierarchical topological and spatial information in graph-

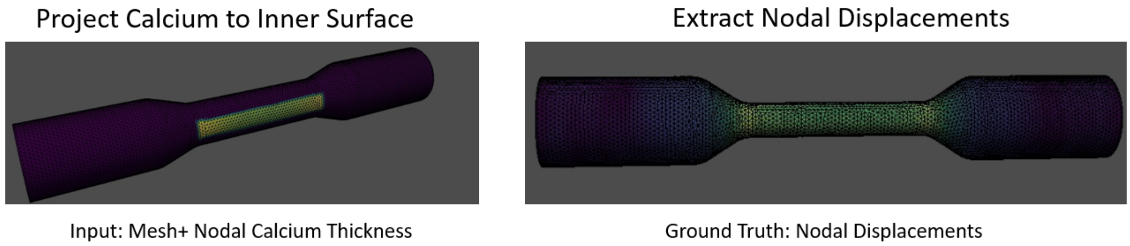

Fig. 3: A visual representation of the input and output representations to be fed into a graph neural network. Left: calcium is projected onto the inner surface of the lumen. Right: The nodal displacements of the inner surface are extracted and used as ground truth to supervise network training.

structured data, enabling the efficient learning of complex patterns across large, densely-connected graphs [4].

The encoder effectively captures both local and global features of the input graph at varying mesh resolutions by employing alternating graph convolutional layers and graph pooling layers. The pooling layer samples a subset of important nodes to facilitate the enlargement of nodal receptive fields [4]. Subsequently, the decoder reconstructs the graph to its original size using a series of graph convolutional layers and unpooling operations. The unpooling layer restores the original graph structure by using the position information of nodes in the original graph and performing the inverse operation of the corresponding pooling layer [4]. To facilitate information transfer across layers, skip connections from the encoding phase are integrated into the decoder. A representation of this architecture, applied to arterial meshes, is presented in Figure 4.

The Graph U-Net architecture is particularly effective at propagating information across the entire mesh structure through its pooling and unpooling operations, unlike traditional graph neural networks that tend to be constrained to a few-hop neighborhood around a node [15]. This ability is particularly important for our vessel expansion problem, as the model must recognize long-range dependencies along the artery to generate physiologically plausible displacement predictions for a given node.

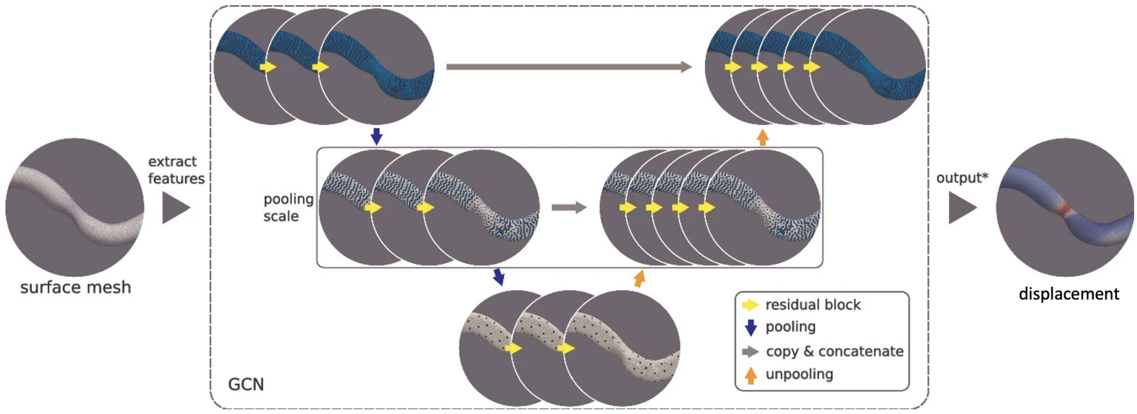

Fig. 4: Graph U-Net architecture used to estimate displacements during coronary angiography. Adapted from [15].

2.6. Experiments. We implement the Graph-UNet architecture using FeaSt convolutions [16], as employed in the existing literature for modeling arterial meshes [15]. A FeaSt convolution [16] represents a graph-convolutional message-passing layer that leverages an attention mechanism to dynamically determine local filters based on the features present in the preceding network layer. The network consists of approximately 800,000 trainable parameters.

Our dataset, comprising 13 arteries, is randomly partitioned into training and testing sets, forgoing a validation set due to data constraints. The graph neural networks are trained to predict a two-dimensional radial displacement vector at each vertex on the surface mesh. All models are trained using a mean absolute error loss and the Adam optimizer. The implementation of this architecture is adapted from the code in [1, 15]. Inference on a new artery featuring unseen mesh geometry requires only a few seconds, as opposed to the equivalent finite element simulation, which took 48 hours.

3. Results. The results are shown below in the following figures. we present the distributions of predicted displacements vs ground truth displacements, and mean absolute error values for the training distribution (Figure 5) and test distribution (Figure 6). The training error increases with the number of training arteries, while the test error trends downwards with the number of training arteries. Indicating the model was overfitting on small datasets but is slowly learning to generalize.

Fig. 5: Consistent distribution of predicted displacements and increasing mean absolute error (MAE) during training as training set (N) grows

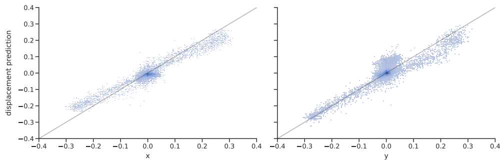

(a) N=1; MAE=0.0248

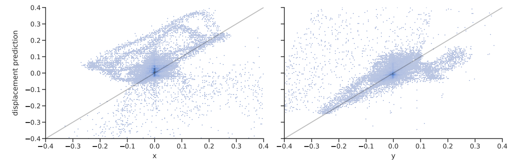

(b) N=3; MAE=0.0736

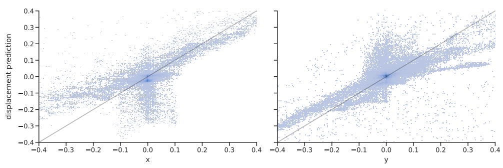

(c) N=6; MAE= 0.0562

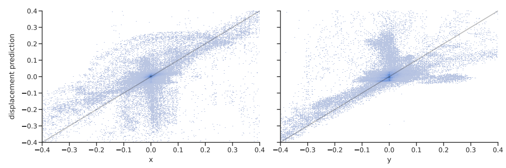

(d) N=9; MAE=0.1181

4. Discussion. In this study, we present a proof of concept for using geometric deep learning to predict vessel expansion during coronary angioplasty, showcasing promising results in the preliminary stage. Our neural network employs geometric deep learning in conjunction with a U-Net architecture, effectively analyzing the 3D arterial mesh to predict radial displacement. Our approach significantly reduces computational time and could potentially enable the real-time prediction of vessel expansion to optimize coronary interventions.

Despite the encouraging results, our training dataset was limited to a mere 13 arteries, which impeded a comprehensive assessment of the graph neural network's performance and its capacity to generalize. To mitigate this limitation, we aim to simulate additional meshes to enhance training and facilitate a more robust evaluation.

Moreover, our current model is not equivariant to transformations in the input data, implying that predictions may be influenced by translations, rotations, or the introduction of noise. To enhance the model's performance, we plan to generate a larger dataset with such augmentations and train the model using this expanded dataset.

Finally, our evaluation in this study relies on a random training and testing split of the dataset. However, in clinical practice, we would prefer to train models on a specific cohort of patients and generalize the model to unseen patients with potentially different morphologies. As a result, future evaluations should take into account data splits based on morphology to gain a deeper understanding of the graph neural network's performance in real-world settings.

Fig. 6: Improving distribution of predicted displacements and decreasing mean absolute error (MAE) during testing as training set (N) grows

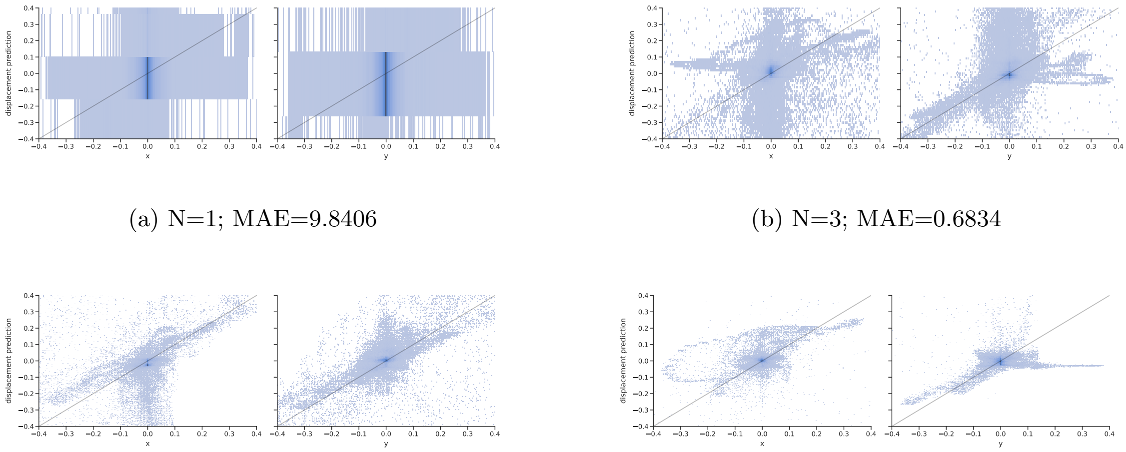

(a) N=1; MAE=9.8406

(b) N=3; MAE=0.6834

(c) N=6; MAE=0.0758

(d) N=9; MAE=0.1213

REFERENCES

[1] P. de Haan, M. Weiler, T. Cohen, and M. Welling, *Gauge equivariant mesh cnns: Anisotropic convolutions on geometric graphs.*

[2] L. L. Demer and Y. Tintut, *Inflammatory, metabolic, and genetic mechanisms of vascular calcification*, Arteriosclerosis, thrombosis, and vascular biology, 34 (2014), pp. 715–723.

[3] A. Fujino, G. S. Mintz, M. Matsumura, T. Lee, S.-Y. Kim, M. Hoshino, E. Usui, T. Yonetsu, E. S. Haag, R. A. Shlofmitz, et al., *A new optical coherence tomography-based calcium scoring system to predict stent underexpansion.*, EuroIntervention: journal of EuroPCR in collaboration with the Working Group on Interventional Cardiology of the European Society of Cardiology, 13 (2018), pp. e2182–e2189.

[4] H. Gao and S. Ji, *Graph u-nets*, in international conference on machine learning, PMLR, 2019, pp. 2083–2092.

[5] J. Gilmer, S. S. Schoenholz, P. F. Riley, O. Vinyals, and G. E. Dahl, *Neural message passing for quantum chemistry*, in ICML, PMLR, 2017, pp. 1263–1272.

[6] G. A. Holzapfel, G. Sommer, C. T. Gasser, and P. Regitnig, *Determination of layer-specific mechanical properties of human coronary arteries with nonatherosclerotic intimal thickening and related constitutive modeling*, American Journal of Physiology-Heart and Circulatory Physiology, 289 (2005), pp. H2048–H2058.

[7] C. H. Lee and S.-H. Hur, *Optimization of percutaneous coronary intervention using optical coherence tomography*, Korean Circulation Journal, 49 (2019), pp. 771–793.

[8] C. D. Mathers and D. Loncar, *Projections of global mortality and burden of disease from 2002 to 2030*, PLoS medicine, 3 (2006), p. e442.

[9] H. Moradi, A. Al-Hourani, G. Concilia, F. Khoshmanesh, F. R. Nezami, S. Needham, S. Baratchi, and K. Khoshmanesh, *Recent developments in modeling, imaging, and monitoring of cardiovascular diseases using machine learning*, Biophysical Reviews, (2023), pp. 1–15.

[10] H. Mori, S. Torii, M. Kutyna, A. Sakamoto, A. V. Finn, and R. Virmani, *Coronary artery calcification and its progression: what does it really mean?*, JACC: Cardiovascular Imaging, 11 (2018), pp. 127–142.

[11] T. Pfaff, M. Fortunato, A. Sanchez-Gonzalez, and P. W. Battaglia, *Learning mesh-based simulation with graph networks*, arXiv preprint arXiv:2010.03409, (2020).

[12] G. Poletti, L. Antonini, L. Mandelli, P. Tsompou, G. S. Karanasiou, M. I. Papafaklis, L. K. Michalis, D. I. Fotiadis, L. Petrini, and G. Pennati, *Towards a digital twin of coronary stenting: A suitable and validated image-based approach for mimicking patient-specific coronary arteries*, Electronics, 11 (2022), p. 502.

[13] L. Räber, G. S. Mintz, K. C. Koskinas, T. W. Johnson, N. R. Holm, Y. Onuma, M. D. Radu, M. Joner, B. Yu, H. Jia, et al., *Clinical use of intracoronary imaging. part 1: guidance and optimization of coronary interventions. an expert consensus document of the european association of percutaneous cardiovascular interventions*, European heart journal, 39 (2018), pp. 3281–3300.

[14] O. Ronneberger, P. Fischer, and T. Brox, *U-net: Convolutional networks for biomedical image segmentation*, in Medical Image Computing and Computer-Assisted Intervention–MICCAI 2015: 18th International Conference, Munich, Germany, October 5-9, 2015, Proceedings, Part III 18, Springer, 2015, pp. 234–241.

[15] J. Suk, P. d. Haan, P. Lippe, C. Brune, and J. M. Wolterink, *Mesh convolutional neural networks for wall shear stress estimation in 3d artery models*, in Statistical Atlases and Computational Models of the Heart. Multi-Disease, Multi-View, and Multi-Center Right Ventricular Segmentation in Cardiac

MRI Challenge: 12th International Workshop, STACOM 2021, Held in Conjunction with MICCAI 2021, Strasbourg, France, September 27, 2021, Revised Selected Papers, Springer, 2022, pp. 93–102.
[16] N. Verma, E. Boyer, and J. Verbeek, *Feastnet: Feature-steered graph convolutions for 3d shape analysis*, in Proceedings of the IEEE conference on computer vision and pattern recognition, 2018, pp. 2598–2606.